J. Fluid Mech. (2000), *vol.* 425, *pp.* 55–77. Printed in the United Kingdom

Oscillatory flow of droplets in capillary tubes. Part 2. Constricted tubes

By D. R. GRAHAM AND J. J. L. HIGDON

Department of Chemical Engineering, University of Illinois, Urbana, IL 61801, USA

(Received 25 June 1999 and in revised form 29 June 2000)

The motion of fluid droplets in constricted capillary tubes is investigated for flows subject to the combined action of a mean pressure gradient and an oscillatory body force. Numerical computations are employed to determine the effect of the oscillatory forcing on the mean flow rate and the mean droplet velocity. In the absence of oscillatory forcing, a critical pressure gradient for droplet propagation exists, below which droplets become plugged in the narrow constrictions of the tube. For mean pressure gradients below this threshold, oscillatory forcing is shown to be an effective means for unplugging the constrictions and remobilizing the droplets. For this remobilization process to occur, the oscillatory forcing level must exceed a specified value, and the oscillatory frequency must remain below a critical frequency. Quasi-steady models are shown to give effective predictions of the unsteady dynamics over a wide range of conditions.

1. Introduction

In Part 1 (Graham & Higdon 2000) of this paper we discussed the use of acoustic stimulation to increase the efficiency of secondary oil recovery operations. We studied droplet motion in straight capillary tubes and showed that acoustic stimulation leads to increased droplet deformation which produces significant increases in the flow rates of both the continuous and dispersed phases. The goal of the present paper is to study droplet flow in a constricted capillary tube to determine the effects of acoustic stimulation on a more realistic model of porous media. The essential feature of this geometry is that significant droplet deformation is required for the droplets to pass through the narrow constrictions. Owing to these constrictions, a minimum forcing level exists below which pore plugging occurs, and the flow rate of both phases approaches zero. A major goal of this paper is to assess the effectiveness of acoustic stimulation in overcoming the pore plugging and enhancing the net transport of the droplet phase.

A number of previous studies have examined the motion of liquid droplets through constricted capillary tubes. In an experimental investigation, Olbricht & Leal (1983) measured the droplet shapes and the extra pressure drop ΔP^+ for a droplet under conditions of constant volume flow rate. They showed that ΔP^+ varies significantly with drop position along the tube, and found that large, high capillary number droplets may experience elongation and breakup. Martinez & Udell (1989) analysed this problem using numerical simulations and confirmed the strong position dependence of ΔP^+. They found that high capillary number flows exhibited pronounced droplet elongation similar to that observed by Olbricht & Leal. Borhan & Hemmat (1997)

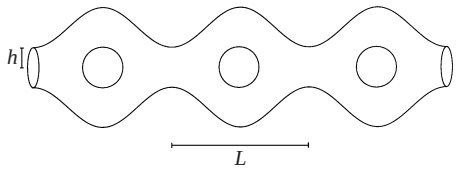

FIGURE 1. Schematic of a constricted capillary tube.

also studied constricted capillary flows, focusing on small drops and evaluating the effects of the capillary geometry (wave amplitude) on ΔP^+.

While the studies above considered a constant volume flow rate, the complementary problem involves a time-dependent flow rate associated with a constant pressure gradient. This problem may be more realistic, because the interconnected nature of real porous media yields flows which are closer to constant pressure gradient than to constant flow rate. Also, this formulation includes the possibility of pore plugging when the imposed pressure gradient is insufficient to force the droplet through the narrowest part of a constriction. Leyrat-Maurin & Barthes-Biesel (1994) studied the flow of a single, liquid-filled capsule moving through a hyperbolic constriction subject to a constant pressure gradient and demonstrated pore plugging below a critical threshold. Hemmat & Borhan (1996) studied the analogous problem for a fluid droplet in a buoyancy-driven flow, determined the velocity of the droplet as a function of Bond number and predicted the critical conditions for droplet breakup.

While the bulk of the research has been restricted to viscous flows, Gauglitz & Radke (1989) considered the flow of a gas bubble through a constriction in the presence of inertial forces. These authors found that viscous flows lead to a slow and steady motion of the bubble through the constriction, while flows dominated by inertia lead to an impulsive motion. For a certain range of parameters, snap-off may occur, leading to bubble breakup and foam generation. In a related study, Tsai & Miksis (1994) showed that snap-off may occur even in Stokes flow if the capillary number is sufficiently small.

On reviewing the literature for flow through constricted capillary tubes, we found no research on the effect of oscillatory forcing on the motion of dispersed fluid droplets. In our investigation of this problem, our goal is to quantify the effect of oscillatory forces on the mean flow rate of both the bulk fluid and droplet phases. We seek to elucidate the fundamental physical mechanisms and thereby to provide a basis for evaluating the relevance of acoustic stimulation for enhanced transport in secondary oil recovery.

2. Problem formulation

We consider the flow of fluid droplets through a periodic constricted channel of sinusoidal profile (figure 1) specified by

$$r = (\alpha + h) + \alpha \sin(kz - \pi/2), \tag{2.1}$$

where $k = 2\pi/L$. The governing equations for a Newtonian fluid are the Navier–Stokes equations and the continuity equation. In Part 1, we specified the governing equations and the boundary conditions appropriate for droplet flow in capillary tubes. We showed that acoustic stimulation is equivalent to an oscillatory body force, while a constant pressure gradient is equivalent to a constant body force. In Part 1 we examined two temporal forcing functions; however in this paper we restrict our

attention to sinusoidal forcing functions with the body force specified by

$$b_z = G_o + G_\omega \sin(2\pi t/\tau), \tag{2.2}$$

where G_ω is the amplitude of the oscillatory force and τ is the period.

The motion of a droplet in a capillary tube is conveniently analysed in a reference frame that moves with the drop. The speed of the reference frame u_{ref} is unknown *a priori* and is determined by adding a constraint equation which specifies the droplet position relative to the origin of the domain:

$$z_{front} + z_{back} = 0, \tag{2.3}$$

where z_{front} and z_{back} are the z-coordinates of the droplet interface evaluated at the centre of the tube. For unsteady problems, this leads to an accelerating reference frame, whose influence is manifested as a body force acting in the negative z-direction with magnitude $\rho(\partial u_{ref}/\partial t)$. This quantity is subtracted from the prescribed body force $b(t)$ to yield the total force $b'(t)$:

$$b'(t) = b(t) - \rho \frac{\partial u_{ref}}{\partial t}. \tag{2.4}$$

Given a reference frame with the drop fixed at the origin, the r-coordinates of the grid points on the boundary wall become functions of time. To update the wall positions, we integrate the frame velocity u_{ref} to obtain the axial displacement relative to the droplet:

$$z_t = \int_0^t u_{ref}\, \mathrm{d}t. \tag{2.5}$$

3. Non-dimensional parameters

In analysing the motion of droplets in constricted tubes, our goal is to determine the flow rate as a function of the tube geometry, forcing conditions, and fluid properties. In this section we introduce the non-dimensional parameters used to characterize these quantities. The geometry is defined by the gap size h, the wall amplitude α, the tube wavelength L, and the drop radius a. These quantities lead to three independent non-dimensional parameters: the pore size h/α, the drop size a/h, and the wall slope αk.

Having specified the geometry, we turn our attention to the characterization of the pressure gradient and the acoustic stimulation. The constant body force G_o representing the mean pressure gradient and the oscillatory body force G_ω representing the acoustic stimulation are non-dimensionalized with the gap size and surface tension yielding dimensionless parameters

$$F_o = G_o h^2/\gamma, \tag{3.1}$$

$$F_\omega = G_\omega h^2/\gamma. \tag{3.2}$$

An equivalent measure of the strength of the oscillatory forcing is the root-mean-square amplitude, which for sinusoidal forcing is

$$F_{rms} = F_\omega/\sqrt{2}. \tag{3.3}$$

The final forcing parameter is the dimensionless frequency based on the period of the

forcing τ and the viscous response time of the droplet $\mu a/\gamma$,

$$f = \frac{\mu a}{\gamma \tau}, \tag{3.4}$$

where μ is the viscosity of the suspending fluid phase. Later in this paper we will discuss the relevant time scales in this problem and show that in certain instances alternative scalings for the frequency prove useful.

The remaining parameters necessary to specify the problem are the fluid properties. As in part 1, the properties of the droplet are defined relative to those of the bulk fluid via the viscosity ratio λ and density ratio ρ_D. The final physical parameter is the material property number

$$Re/Ca = \frac{\rho \gamma h}{\mu^2}. \tag{3.5}$$

The geometry, forcing, and fluid properties are sufficient to determine both the droplet velocity U_{drop} and the bulk fluid velocity U. The bulk velocity is calculated by averaging over the cross-sectional area at the narrowest part of the tube, hence

$$U = \frac{1}{\pi h^2} \int_0^h \boldsymbol{u} \cdot \boldsymbol{n}\, 2\pi r \, \mathrm{d}r. \tag{3.6}$$

Note that different choices for the axial position of the averaging cross-section would lead to smaller values for U. The bulk fluid velocity is non-dimensionalized by defining the capillary number

$$Ca = \mu U/\gamma. \tag{3.7}$$

For flow in constricted tubes, both the bulk fluid velocity and the droplet velocity are functions of time; therefore mean quantities are useful:

$$\bar{U} = \lim_{t_2 \to \infty} \frac{1}{t_2 - t_1} \int_{t_1}^{t_2} U(t)\, \mathrm{d}t, \tag{3.8}$$

$$\bar{U}_{drop} = \lim_{t_2 \to \infty} \frac{1}{t_2 - t_1} \int_{t_1}^{t_2} U_{drop}(t)\, \mathrm{d}t. \tag{3.9}$$

The mean bulk velocity is non-dimensionalized via the mean capillary number

$$\overline{Ca} = \mu \bar{U}/\gamma. \tag{3.10}$$

For constant forcing, an alternative measure of the mean velocity is the dimensionless permeability

$$\kappa = \frac{\bar{U}\mu}{G_o h^2}. \tag{3.11}$$

For flows with both a mean and an oscillatory forcing component, we find it convenient to scale the mean flow rate $\bar{U}$ with the bulk fluid velocity U_1 for single-phase flow at the same mean forcing level F_o. Also, we find the relative droplet velocity $\bar{U}_{drop}/\bar{U}$ to be a useful measure of the droplet velocity.

For many multiphase flows, one is interested in the ratio of the volumetric flow rate of the drop phase to the total flow rate. The flow rate of droplets is $Q_{drop} = \frac{4}{3}\pi a^3 \bar{U}_{drop}/L$, while the total flow rate is $Q = \pi h^2 \bar{U}$. Thus, the ratio of the volume

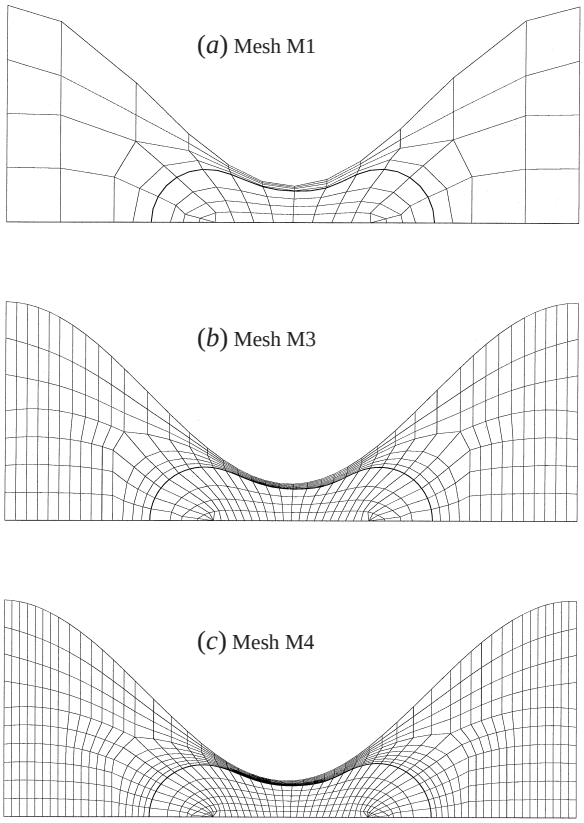

FIGURE 2. Drop profiles for three different meshes. The conditions are drop size $a/h = 2$, property number $Re/Ca = 0$, viscosity ratio $\lambda = 1$, density ratio $\rho_D = 1$, and forcing level $F_o = 0.18$.

Mesh	Number of elements	Bulk	Droplet
M1	104	0.067763	0.013220
M2	136	0.066267	0.012944
M3	424	0.066133	0.012921
M4	808	0.066130	0.012921

TABLE 1. Effect of mesh refinement on the bulk fluid flow rate and the drop flow rate for four different meshes. Columns show dimensionless velocities $\mu\bar{U}/\gamma$ and $\mu\bar{U}_{drop}/\gamma$ respectively.

flow rates is related to the relative droplet velocity by a simple expression:

$$\frac{Q_{drop}}{Q} = \frac{4a^3}{3Lh^2}\frac{\bar{U}_{drop}}{\bar{U}}. \tag{3.12}$$

In reservoir models, one is often interested in the relative permeability of the two fluid phases. The relative permeability (drop phase versus bulk) for our simple system is exactly equal to the ratio of volume flow rates given here. Thus the relative permeability is directly proportional to the relative drop velocity.

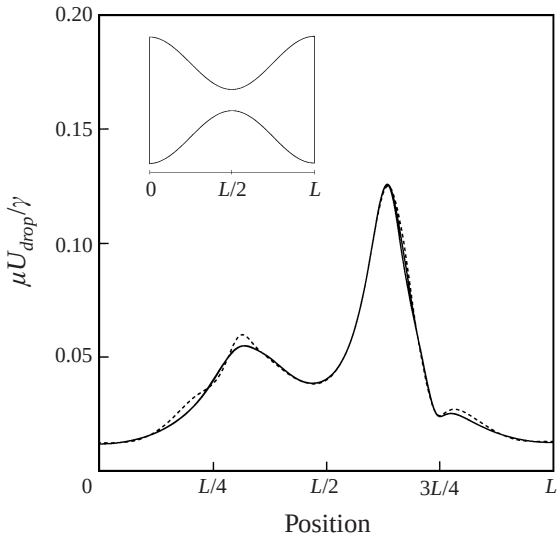

FIGURE 3. Drop velocity as a function of position for four different levels of grid refinement. The dotted line represents mesh M1, the solid lines represent meshes M2–M4. Conditions are drop size $a/h = 2$, property number $Re/Ca = 0$, viscosity ratio $\lambda = 1$, density ratio $\rho_D = 1$, and forcing level $F_o = 0.18$.

4. Numerical methods

The governing equations and boundary conditions are solved with the Galerkin finite element method. Details of our implementation of this method are described in Part 1 and in Graham (1999). In this section, our goal is to verify the accuracy of this method for droplet flow in constricted tubes. In figure 2, we present drop profiles for three different levels of mesh refinement, and we observe that the profiles are very similar for each mesh. Furthermore, as shown in table 1, the mean bulk flow rate and the mean droplet velocity vary by less than 0.25% between meshes M2 and M4. As a final accuracy test, figure 3 shows the instantaneous drop velocity as a function of position along the tube. Meshes M2–M4 are denoted by solid lines and show nearly identical behaviour, while only the coarsest mesh M1 (dotted line) deviates significantly. Given the similarity between meshes M2–M4 in the calculated drop shapes, mean flow rates, and droplet velocity as a function of position, mesh M3 will be used for the majority of the calculations presented here. We note that mesh M2 is probably sufficient for accuracy purposes, but we have found that using a slightly higher level of mesh refinement allows the resolution of a wider range of droplet shapes without excessive mesh distortion or grid point overlap.

5. Results for constant forcing level

Our primary goal in this paper is to determine the effect of oscillatory forcing on the droplet motion and the bulk flow rate in constricted capillary tubes. Before addressing this problem, we must first characterize the behaviour of these flows subject to a constant pressure gradient or body force. These results will provide a basis from which to evaluate the effects of oscillatory forcing.

For droplet motion at arbitrary capillary number, the drop shape and velocity will depend upon the drop response as it passes through a number of successive

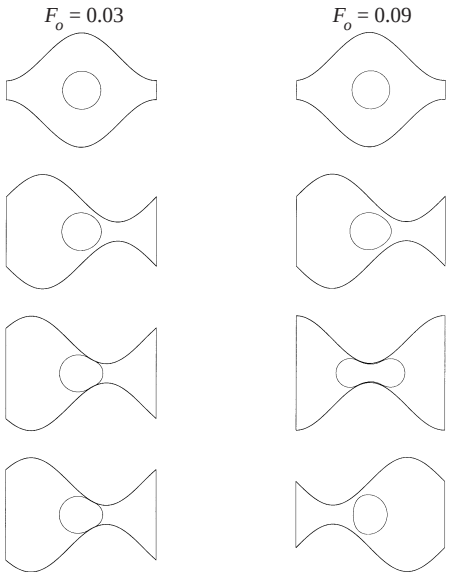

FIGURE 4. Drop profiles for different positions along the tube for two different forcing levels. Conditions are property number $Re/Ca = 0$, drop size $a/h = 2$, viscosity ratio $\lambda = 1$, and density ratio $\rho_D = 1$.

constrictions in the capillary tube. Both the drop velocity and the bulk velocity will be functions of the droplet deformation history. Neither quantity is necessarily a periodic function of time or position, despite the periodicity of the capillary geometry. In the present section, we shall restrict our attention to droplets with small capillary numbers for which the response time of the droplet is small compared with the time scale for convective motion. The viscous and inertial response times of the droplet are $\mu a/\gamma$ and $\sqrt{\rho a^3/\gamma}$ respectively, while the convective time scale is L/U. Taking the ratio of these scales, we require

$$\left(Ca\frac{a}{L}\right) \ll 1 \quad \text{and} \quad (Re/Ca)^{1/2}\left(Ca\frac{a}{L}\right) \ll 1. \tag{5.1}$$

(The Reynolds number based on the ratio of time scales is $\rho Ua/\mu$ however $a/h \approx 1$.) Under these conditions, the droplet shape, droplet velocity and bulk velocity are uniquely determined by the instantaneous droplet position and the forcing level in the capillary. All quantities are periodic functions of position and time. In § 6 below, we shall see that this simplification proves extremely useful in the development of a quasi-steady theory for analysis of oscillatory forcing.

In the remainder of this section, we first determine the effects of forcing level on the drop profiles, the instantaneous flow rates and the permeability. We then determine the permeability for a wide range of drop sizes, material property numbers and viscosity ratios. The results presented in this paper will be limited to a capillary with $\alpha k = 1$ and $h/\alpha = 0.4$; however, results for other tube geometries are given in Graham (1999).

5.1. *Forcing level effects*

We begin our presentation by examining the effects of forcing level on droplet flow in constricted tubes. Figure 4 shows drop profiles at different positions along the tube for two different forcing levels. For the lowest forcing level, the force is insufficient to

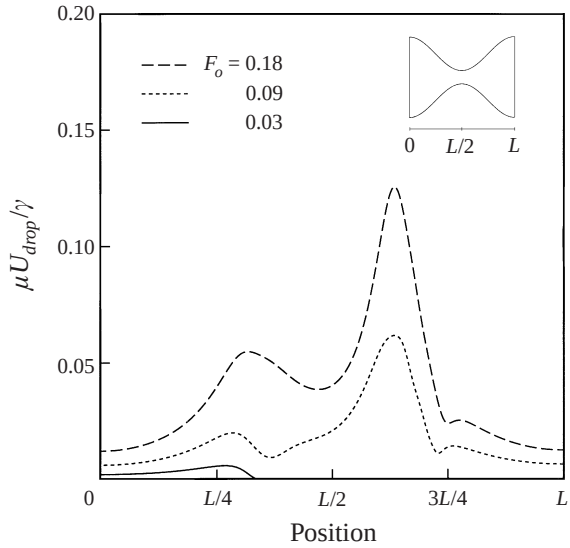

FIGURE 5. Drop velocity as a function of position for different forcing levels. Conditions are property number $Re/Ca = 0$, drop size $a/h = 2$, viscosity ratio $\lambda = 1$, and density ratio $\rho_D = 1$.

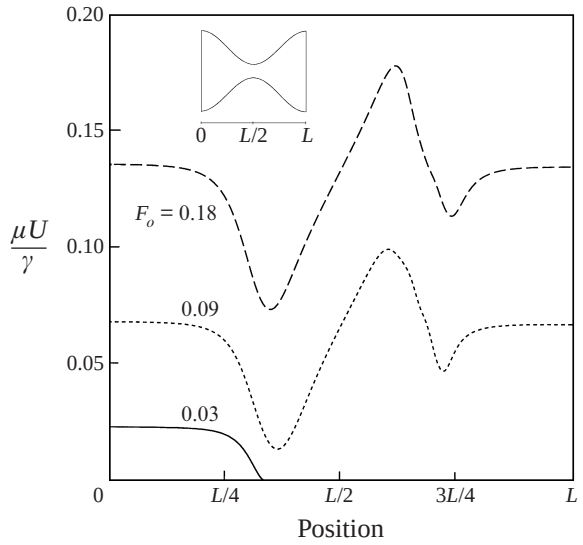

FIGURE 6. Bulk flow rate as a function of position for different forcing levels. Conditions are $Re/Ca = 0$, drop size $a/h = 2$, viscosity ratio $\lambda = 1$, and density ratio $\rho_D = 1$.

push the drop through the narrow part of the constriction and pore plugging occurs. For the higher forcing level, the force is strong enough to overcome surface tension forces and the drop passes through the constriction. The effects of forcing level on the instantaneous droplet velocity are shown in figure 5. At the lowest forcing level ($F_o = 0.03$) the drop velocity approaches zero near position $L/3$ as pore plugging occurs. At higher forcing levels no plugging occurs, and the drop velocity increases as it moves from the wide part of the tube and approaches the constriction. Owing to mass conservation, the local fluid velocity increases as the tube narrows, which

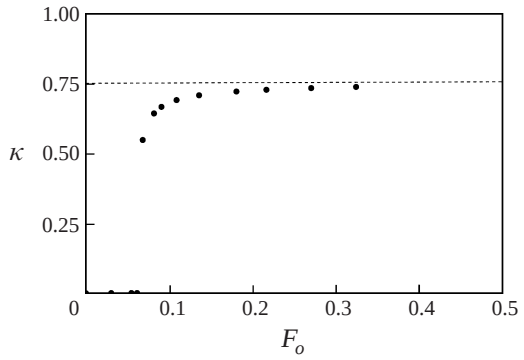

FIGURE 7. Permeability as function of force for property number $Re/Ca = 0$, drop size $a/h = 2$, viscosity ratio $\lambda = 1$, and density ratio $\rho_D = 1$.

increases the droplet velocity. The droplet slows slightly as it enters the narrowest part of the tube, with the increased resistance arising from the energy required for droplet deformation. Upon exiting the narrowest region, the drop expands, releasing surface energy which propels the drop out of the constriction and increases its velocity.

Turning our attention to the bulk flow rate (figure 6), we observe that it approaches zero for the lowest forcing level $F_o = 0.03$ owing to pore plugging. For higher forcing levels, the bulk flow rate decreases sharply as the drop enters the constriction, but then increases dramatically as the drop exits the constriction. This is a reflection of the same phenomenon seen for the droplet velocity. As a droplet enters a constriction, the deformation of the interface leads to large storage of interfacial energy. When the droplet leaves the constriction, the release of this energy pushes the droplet forward yielding the rapid acceleration seen in the figure. At the end of this stage, the droplet assumes a nearly constant shape, and the bulk flow rate changes little as the drops transits the expanded portion of the capillary.

Given that the bulk flow rate and droplet velocity vary with position and time for these flows, the relevant measures of the overall flow rate are the mean bulk flow rate $\bar{U}$ and the mean droplet velocity $\bar{U}_{drop}$. These quantities are conveniently characterized by the permeability κ and the relative droplet velocity $\bar{U}_{drop}/\bar{U}$. Figure 7 shows the permeability as a function of forcing level. For low forcing levels, the permeability is nearly zero owing to pore plugging. As the forcing level passes the critical value for droplet flow F_{plug}, the permeability increases sharply. Further increases in the forcing level lead to a relatively constant permeability that approaches the level for single-phase flow (dotted line). This indicates that the droplet has a small effect on the permeability for forcing levels higher than roughly twice the value F_{plug}. The mean capillary number for these flows is given by the relationship $\overline{Ca} = \kappa F_o$. The capillary numbers for the forcing levels in figure 7 range from 0 to 0.25, with a value of order $\overline{Ca} \approx 0.04$ at the plugging threshold.

Figure 8 shows the relative droplet velocity as a function of forcing level. Its small value (≈ 0.2) reflects the fact that the bulk fluid velocity is defined at the narrowest portion of the tube. The relative droplet velocity is essentially constant with respect to forcing level, and therefore the following discussion will focus primarily on the bulk flow rate. Detailed results for the droplet velocity are given in Graham (1999).

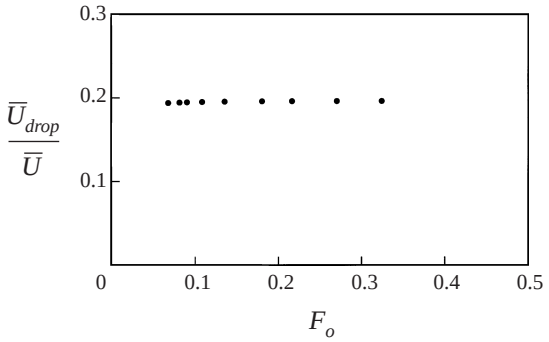

FIGURE 8. Relative droplet velocity as function of force for property number $Re/Ca = 0$, drop size $a/h = 2$, viscosity ratio $\lambda = 1$, and density ratio $\rho_D = 1$.

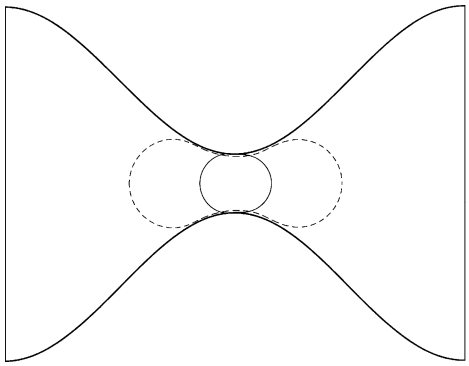

FIGURE 9. Drop profiles for two different size droplets; the dotted line is $a/h = 2$ and $F_o = 0.09$, and the solid line is $a/h = 1.1$ and $F_o = 0.0125$. Other conditions are $Re/Ca = 0$, $\lambda = 1$, density ratio $\rho_D = 1$.

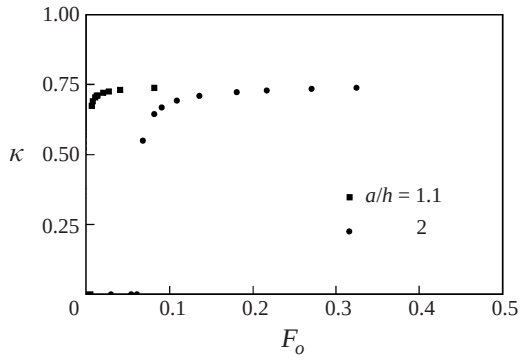

FIGURE 10. Permeability as function of force for two different drop sizes. Conditions are property number $Re/Ca = 0$, viscosity ratio $\lambda = 1$, and density ratio $\rho_D = 1$.

5.2. *Drop size effects*

The next parameter considered is drop size. In figure 9 we compare the drop profiles at the narrow portion of the tube for two different drop sizes. For the smaller drop size $a/h = 1.1$, significantly less deformation is required for the droplet to pass through the constriction compared with drops of size $a/h = 2$. Figure 10 shows the permeability as

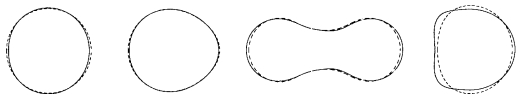

FIGURE 11. Drop profiles for two different material property numbers; the dotted lines are $Re/Ca = 0$ and the solid lines are $Re/Ca = 500$. The conditions are drop size $a/h = 2$, viscosity ratio $\lambda = 1$, density ratio $\rho_D = 1$, and $F_o = 0.09$.

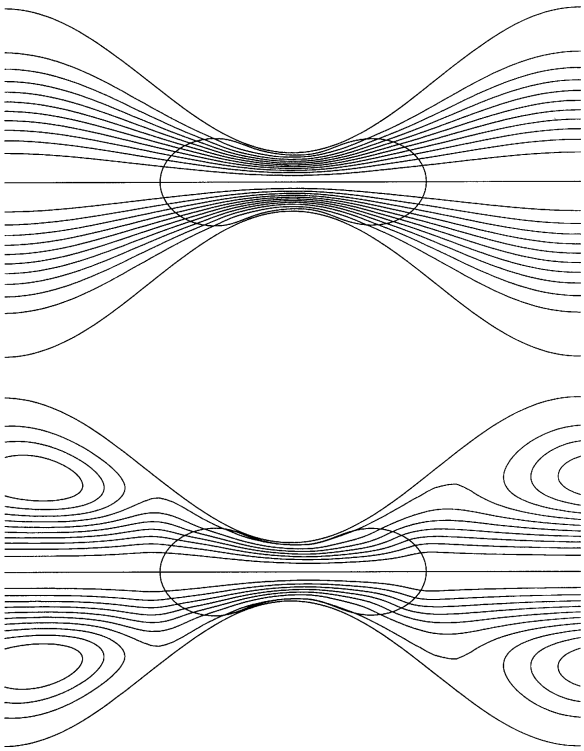

FIGURE 12. Streamline patterns for flow at (*a*) $Re/Ca = 0$ and (*b*) $Re/Ca = 500$. Conditions are drop size $a/h = 2$, viscosity ratio $\lambda = 1$, density ratio $\rho_D = 1$, and $F_o = 0.09$.

a function of forcing level for both drop sizes. While the plugging threshold is much lower for $a/h = 1.1$ than for $a/h = 2$, both curves exhibit similar shapes with a region of negligible permeability rising quickly to a region of relatively constant permeability as the forcing level increases. In each case, there is little effect on permeability for forcing levels above two times F_{plug}.

5.3. *Inertial effects*

While the previous sections have been restricted to purely viscous flow, in this section we consider flows for which inertial effects are present. The parameter that measures the relative importance of inertial effects is the material property number Re/Ca. In figure 11, we compare typical drop profiles for $Re/Ca = 0$ to those for $Re/Ca = 500$ for a droplet at successive locations within the tube. The profiles in this figure correspond to the droplet positions illustrated previously in figure 4. For the droplet which has exited the constriction (profile at far right), the rear of the drop with $Re/Ca = 500$ is flatter than that for $Re/Ca = 0$. This flatter shape arises as the droplet exits the constriction. The rear of the droplet moves faster than the front,

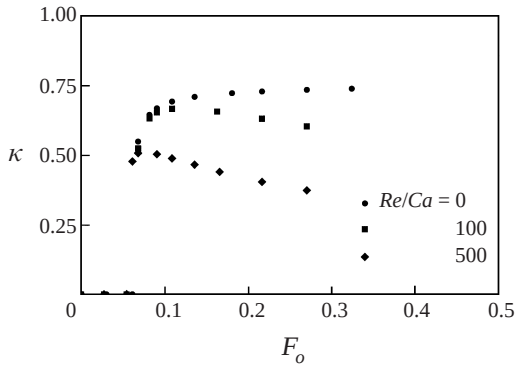

FIGURE 13. Permeability as function of force for different property numbers. Conditions are drop size $a/h = 2$, viscosity ratio $\lambda = 1$, and density ratio $\rho_D = 1$.

and its high velocity is sustained by the fluid inertia. While the droplet profiles show relatively subtle changes in shape, the streamline patterns in figure 12 show marked contrast for the two property numbers. For the $Re/Ca = 0$ case, the streamlines contract in the narrow part of the tube and expand in the wider section similar to those for single-phase flow at low Reynolds number. For the $Re/Ca = 500$ case, a concentrated jet of fluid forms in the centre of the capillary with recirculating vortices in the expanded regions of the channel. The instantaneous Reynolds number ($Re = \rho Uh/\mu$) for this flow is 20.3. Flow patterns of this type are common for single-phase flows in constricted channels at comparable Reynolds number (Graham 1997).

Turning our attention from the drop profiles and streamline patterns to the effects of inertia on permeability, we plot the permeability as a function of forcing level for three different values of Re/Ca in figure 13. As the property number Re/Ca increases from 0 to 500, the plugging threshold F_{plug} decreases slightly. In a purely viscous flow, the droplet becomes plugged when the pressure force is balanced by strong surface tension forces. For inertial flows, however, the droplet tends to remain in motion even when these two forces balance, and this extra inertia provides the impetus needed to pass through the constriction. Inertial effects are also apparent in the dependence of the permeability on forcing level for relatively high forcing ($F_o > F_{plug}$). Here, for both $Re/Ca = 100$ and $Re/Ca = 500$, the permeability *decreases* as the forcing level increases. An analogous trend is observed for single-phase flow: the permeability is constant for $Re = 0$, while it decreases for finite Reynolds number flows due to inertial drag. In figure 14, we show the relative droplet velocity as a function of forcing level for each material property number. The relative droplet velocity is nearly constant for $Re/Ca = 0$, while it increases with forcing level for larger material property numbers. This dramatic increase is due to the jet of fluid that forms in the centre of the channel for inertial flows. At high Re, the concentrated jet carries the droplet through the expanded portion of the capillary at velocities approaching the level of the bulk velocity in the constriction.

5.4. *Viscosity ratio effects*

Effects of viscosity ratios other than $\lambda = 1$ are considered in detail in Graham (1999). The plugging threshold is not a strong function of viscosity ratio, but the permeability for higher forcing level was found to decrease with increases in viscosity ratio.

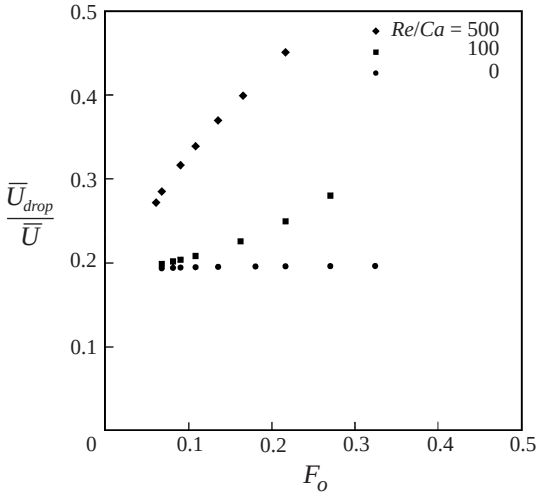

FIGURE 14. Relative droplet velocity as function of force for different property numbers. Conditions are drop size $a/h = 2$, viscosity ratio $\lambda = 1$, and density ratio $\rho_D = 1$.

6. Quasi-steady analysis

In this section, we develop a quasi-steady model to predict the system response to oscillatory forcing based on data from simulations with constant forcing levels. The quasi-steady model has much lower computational cost compared with full unsteady simulations, and it gives effective predictions for the flow behaviour over a wide range of conditions.

For droplet flow in constricted tubes with oscillatory forcing, there are five distinct time scales: the viscous and inertial response times of the droplet $\mu a/\gamma$ and $\sqrt{\rho a^3/\gamma}$, the viscous diffusion time $\rho h^2/\mu$, the period of the oscillatory forcing τ and the convective time scale for the periodic geometry L/U_1. The first four time scales have been encountered previously in Part 1. As in that study, the first requirement for a quasi-steady model is that the droplet response times and viscous diffusion time be much smaller than the period τ. As before, this leads to the constraints

$$f \ll 1, \quad f\sqrt{Re/Ca} \ll 1, \quad f(Re/Ca) \ll 1. \tag{6.1}$$

In addition to these constraints, an efficient quasi-steady model requires that the velocity can be specified as a unique function of position and instantaneous forcing level, independent of deformation history. In the previous section we found that this condition is satisfied if the response time of the droplet is small relative to the convective time scale, which requires

$$\left(Ca\frac{a}{L}\right) \ll 1 \quad \text{and} \quad (Re/Ca)^{1/2}\left(Ca\frac{a}{L}\right) \ll 1. \tag{6.2}$$

When these conditions are satisfied, the results of the constant-forcing simulations of § 5 may be employed to give quasi-steady predictions of the bulk flow rate and drop velocity in the presence of oscillatory forcing. The instantaneous velocity is given by

$$U(t) = U_o(z(t); F)\,|_{F=F(t)}, \tag{6.3}$$

in which $U(t)$ and U_o represent either the bulk fluid velocity or the droplet velocity, and $U_o(z(t); F)$ is the velocity at position $z(t)$ for given constant forcing level F. The

mean flow is computed as

$$\bar{U} = \lim_{t_2 \to \infty} \frac{1}{t_2 - t_1} \int_{t_1}^{t_2} U_o(z(t); F(t))\, \mathrm{d}t. \tag{6.4}$$

The final parameter which affects the quasi-steady analysis is the ratio of the convective time scale to the oscillatory period. We shall call the ratio $L/U_1\tau$ the periodic frequency. For periodic frequency $L/U_1\tau \ll 1$, the oscillatory forcing shows negligible change as the droplet passes through many constrictions. For periodic frequency $L/U_1\tau \gg 1$, the droplet experiences many cycles of oscillatory forcing with negligible change in mean axial position. The quasi-steady prediction (6.4) is valid for arbitrary periodic frequency, because it specifically incorporates the position dependence in computing the velocity. In general, the integration in (6.4) requires integration over many oscillatory forcing cycles, because the disparate time scales in the spatial dependence $z(t)$ and temporal dependence $F(t)$ yield a velocity which is not periodic in time. In the limit of small periodic frequency however, the integral may be computed in simpler fashion. In this case, the droplet travels through many constrictions at a given forcing level, and we infer that the relationship between $U(t)$ and $F(t)$ is identical to that between $\bar{U}$ and F_o for simulations with a constant force. Thus we may average $\bar{U}(F_o)$ over all forcing levels in one cycle to obtain the quasi-steady prediction of the mean flow rate.

The data for quasi-steady predictions require a series of simulations at different constant forcing levels. For each forcing level, we compute and tabulate the drop velocity and the bulk fluid velocity as a function of drop position along the tube. To predict the velocity at an arbitrary position and forcing level, we perform two interpolations. First, we interpolate to find the velocity at the current droplet position for each constant forcing level. Next, we interpolate these data with respect to the forcing level to find the velocity at the appropriate position and instantaneous forcing level. With this procedure, we may then integrate (6.4) over many periods to evaluate the mean velocities.

7. Quasi-steady results

In this section, we present results for the quasi-steady analysis of oscillatory forcing. We first examine low periodic frequencies to determine the mean flow rate and the mean droplet velocity for a wide range of forcing conditions, geometric parameters and fluid properties. For a given set of parameters, we then explore periodic frequency effects in an effort to determine the range of frequencies for which these trends hold.

7.1. *Oscillatory forcing level*

We begin by considering the effects of forcing level on the mean flow rate. Figure 15 shows the mean flow rate as a function of oscillatory forcing level. For this plot, the periodic frequency is small ($L/U_1\tau \to 0$) and the specified mean force is below the threshold required to push the droplet through the constrictions ($F_o < F_{plug}$). For low levels of oscillatory forcing, the flow rate is very small due to pore plugging. As the oscillatory forcing level increases, we reach a point at which the instantaneous force is strong enough to drive the droplet through the constriction. Once this threshold is reached, the flow rate increases dramatically. Further increases in the forcing level cause the mean flow rate to decrease slightly before levelling off. The shape of this plot can be understood in the context of figure 16, which shows an idealized version of the mean velocity as a function of constant forcing level. In regions 1 and 4 the

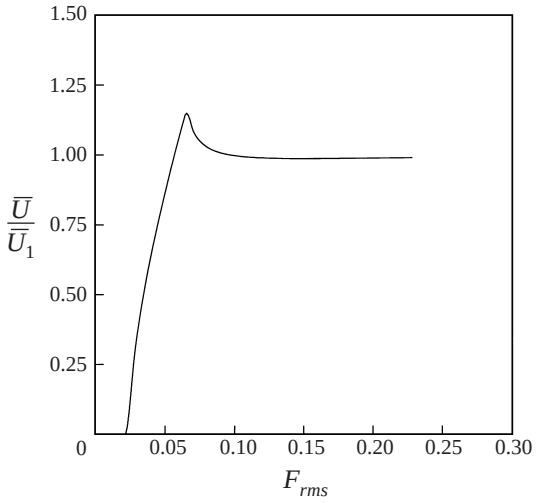

FIGURE 15. Quasi-steady analysis showing mean flow rate vs. oscillatory forcing where the steady forcing is below plugging threshold. Conditions are property number $Re/Ca = 0$, drop size $a/h = 2$, viscosity ratio $\lambda = 1$, density ratio $\rho_D = 1$, $F_o = 0.03$, and $L/U_1\tau \to 0$.

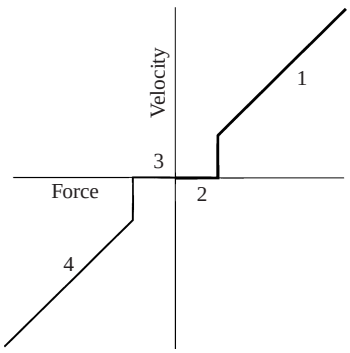

FIGURE 16. Schematic representation of force vs. velocity for constricted tube.

permeability is constant (velocity vs. force is linear), and in regions 2 and 3 plugging occurs. For the quasi-steady results shown in figure 15, the steady component of the force is in region 2 (plugging), and the sharp increase in mean flow rate occurs when the positive portion of the oscillatory forcing cycle samples region 1 (linear) and the negative portion samples region 3 (plugging). As the oscillatory forcing becomes stronger, the negative portion of the forcing cycle samples region 4 (linear) and the mean flow rate decreases. For strong oscillatory forcing, the mean bulk velocity is comparable to the flow rate for a single-phase fluid at the same forcing level F_o. This indicates that the addition of the oscillatory forcing to a plugging capillary flow not only mobilizes the droplets but also reduces the droplet resistance enough to generate a significant mean flow rate.

Moving from systems with a mean force below the plugging threshold to systems with a mean force greater than F_{plug}, figure 17 shows the mean flow rate as a function of oscillatory forcing for conditions where F_o is about 50% larger than F_{plug}. For low oscillatory forcing levels, we observe a decrease in mean flow rate, which can be understood in the context of figure 16. The steady component of the force is in the

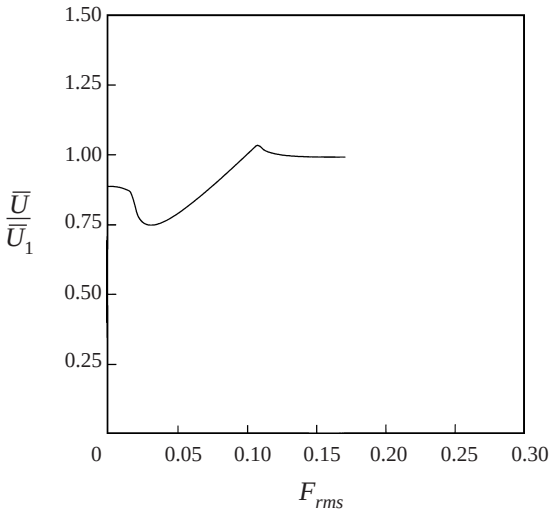

FIGURE 17. Quasi-steady analysis showing mean flow rate vs. oscillatory forcing where the steady forcing is above the plugging threshold. Conditions are property number $Re/Ca = 0$, drop size $a/h = 2$, viscosity ratio $\lambda = 1$, density ratio $\rho_D = 1$, $F_o = 0.09$, and $L/U_1\tau \to 0$.

linear region of the plot (region 1). As a small oscillatory force is added, the positive portion of the forcing cycle samples the linear region (region 1), whereas the negative portion of the cycle moves the net force into the plugging region 2. The pore plugging during this interval yields a smaller flow rate than that for constant permeability and decreases the mean flow rate. For stronger oscillatory forcing, there is a slight increase in the mean flow rate. For this case, a portion of the negative forcing interval samples region 3 (plugging) yielding negligible reverse flow, and the mean flow rate is higher as a result. While oscillatory forcing has some effect on the mean flow rates for $F_o > F_{plug}$, the change is small compared to systems where $F_o < F_{plug}$; for the rest of this paper we will focus on systems with $F_o < F_{plug}$.

7.2. *Drop size effects*

Having shown that oscillatory forcing can enhance the mean flow rate for a droplet of given size, we now consider the effect of varying the drop size. Figure 18 shows the mean flow rate as a function of oscillatory forcing level for two different drop sizes. For the smaller drops, a lower force is required to generate a mean flow, consistent with the results for the plugging threshold discussed previously (§ 5.2). Despite the difference in threshold values, the mean flow rate is very similar for the two drop sizes at oscillatory forcing levels proportionately above the respective values of F_{plug}. For droplets smaller than those considered here (e.g. $a/h < 1$), very little deformation occurs, and oscillatory forcing has only a slight effect on the mean flow rate.

7.3. *Inertial effects*

In this subsection, we evaluate the effects of fluid inertia on the enhancement in mean flow rate. Figure 19 shows the mean bulk velocity as a function of oscillatory forcing level for two values of Re/Ca. The primary difference between the curves for the two property numbers is the decrease in bulk flow rate at high forcing levels for $Re/Ca = 500$. This decrease arises due to the nonlinear inertial drag and is to be expected based on the constant-forcing results shown in figure 13. In figure 20, we show the results for the droplet velocity. In contrast to the bulk fluid flow rate, the

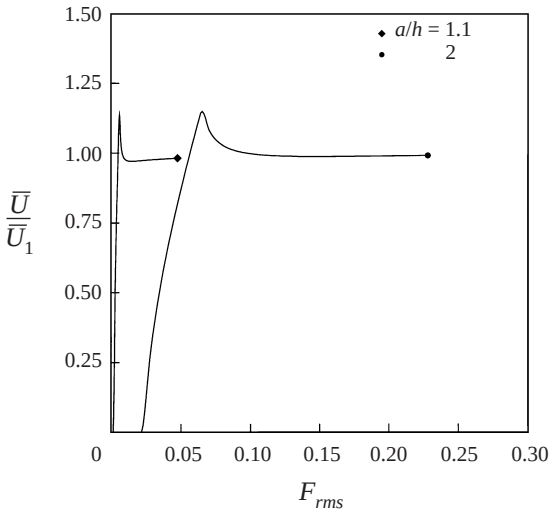

FIGURE 18. Quasi-steady analysis showing mean flow rate vs. oscillatory forcing for different drop sizes and where the steady forcing is below the plugging threshold. Conditions are property number $Re/Ca = 0$, viscosity ratio $\lambda = 1$, density ratio $\rho_D = 1$, and $L/U_1\tau \to 0$. The steady force for both drop sizes is about half of the plugging threshold; $F_o = 0.03$ for $a/h = 2$ and $F_o = 0.003$ for $a/h = 1.1$.

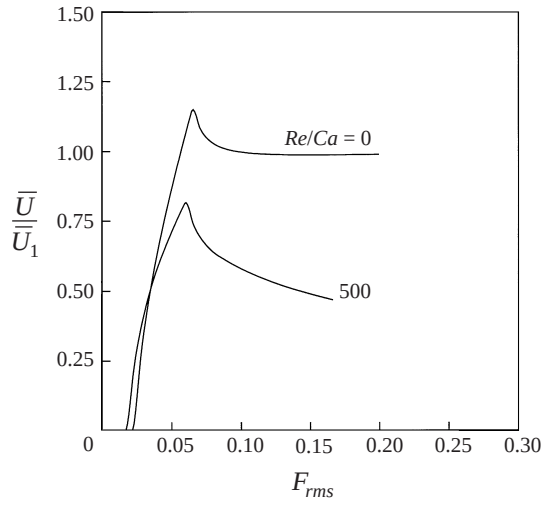

FIGURE 19. Quasi-steady analysis showing mean flow rate vs. oscillatory forcing for different levels of Re/Ca and where the steady forcing is below the plugging threshold. Conditions are drop size $a/h = 2$, viscosity ratio $\lambda = 1$, density ratio $\rho_D = 1$, $F_o = 0.03$, $L/U_1\tau \to 0$.

mean droplet velocity increases monotonically with increasing forcing level, even for large F_{rms}. This trend is expected based on the constant-forcing results which show the formation of a concentrated jet of fluid in the centre of the channel. A distinctive feature of inertial flows is that the oscillatory force can act both to overcome pore plugging and to increase the relative droplet velocity. In contrast, for more viscous flows the oscillatory forcing serves to overcome pore plugging, but has little effect on the relative droplet velocity.

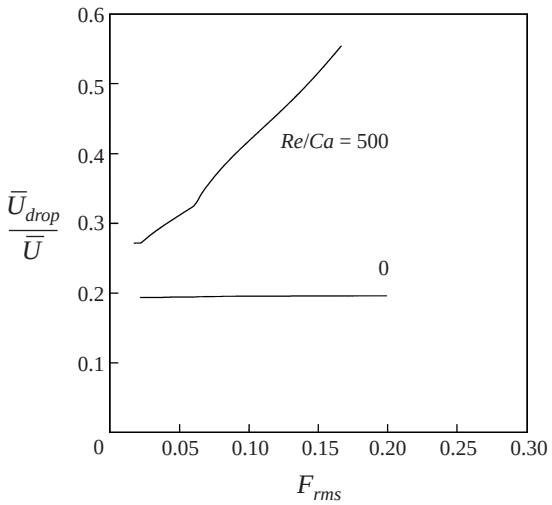

FIGURE 20. Quasi-steady analysis showing relative droplet velocity vs. oscillatory forcing for different levels of Re/Ca and where the steady forcing is below the plugging threshold. Conditions are drop size $a/h = 2$, viscosity ratio $\lambda = 1$, density ratio $\rho_D = 1$, $F_o = 0.03$, $L/U_1\tau \to 0$.

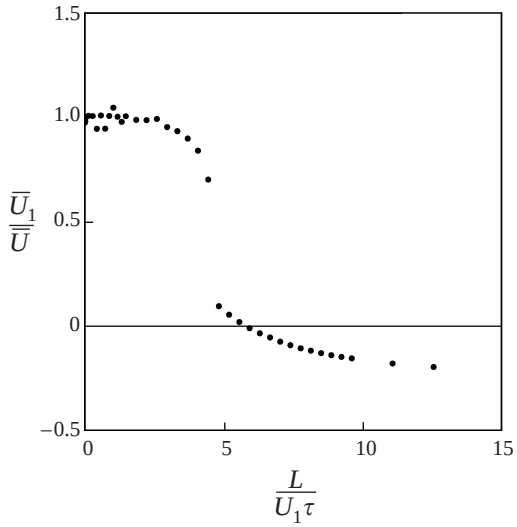

FIGURE 21. Quasi-steady analysis showing mean flow rate vs. frequency of forcing for a case where steady forcing is below plugging threshold. Conditions are property number $Re/Ca = 0$, drop size $a/h = 2$, viscosity ratio $\lambda = 1$, density ratio $\rho_D = 1$, $F_o = 0.03$, and $F_{rms} = 0.15$.

7.4. *Viscosity ratio effects*

Quasi-steady results for three different viscosity ratios are presented in Graham (1999). The effects of viscosity ratio on quasi-steady analysis are similar to those for constant forcing.

7.5. *Periodic frequency effects*

The final parameter we consider is the periodic frequency $L/U_1\tau$. Recall that quasi-steady analysis can be employed to capture periodic frequency effects for conditions where the droplet response and viscous diffusion time scales are small (equations

(6.1), (6.2)). To investigate periodic frequency dependence, we select a typical set of conditions with a mean forcing level F_o below the plugging threshold F_{plug} and an oscillatory forcing level F_{rms} five times that of the mean force. The mean flow rate as a function of periodic frequency is shown in figure 21. For frequencies up to $L/U_1\tau \approx 3$, the oscillatory forcing overcomes the plugging threshold and generates a significant mean flow comparable to that achieved at the low-frequency limit. When the periodic frequency $L/U_1\tau \approx 5$, the mean flow rate decreases dramatically. For the lower frequencies, the instantaneous forcing level remains above the plugging threshold for a significant length of time and allows the droplet to flow through the constriction. As the periodic frequency increases however, the time interval during a single cycle is insufficient, and additional cycles are required to drive the droplet through the constriction. At high enough frequency, the time intervals are too short and the droplet remains immobilized on the upstream side of the constriction. Although the droplet is immobilized, the oscillatory forcing still has an interesting effect on the bulk flow rate. During the positive portion of the forcing cycle, the droplet is pushed firmly against the constriction, leaving a very small gap and negligible forward flow rate. During the negative portion of the cycle, the droplet is pushed *away* from the constriction, producing a larger gap and allowing significant flow in the negative direction. In effect, the immobilized droplet acts as a one-way flow valve for the oscillatory driving force. The net result is that a significant mean flow is generated in the direction *opposite* to that of the mean driving force.

Having shown that significant positive flow enhancement occurs for frequencies below a certain critical value, we now focus on how this critical frequency varies with oscillatory forcing level. We define the critical frequency by the condition that a droplet moves freely through constrictions for subcritical frequencies, but is immobilized for frequencies above the critical value. In computing this critical frequency, our numerical criterion for an immobilized droplet is that the mean droplet velocity remains below 2% of the low-frequency asymptotic value for 10 cycles of oscillatory forcing. Alternatively, if the droplet passes the midpoint of the constriction at $0.5L$, we assume that it is mobilized. Using these criteria, calculations were repeated at different frequencies until the critical frequency was bracketed with an uncertainty of 2%. Figure 22 shows the computed values for the critical frequency as a function of the oscillatory forcing level. As the forcing level increases, the critical frequency increases in a nearly linear fashion with a levelling trend at the upper end near $L/U_1\tau \approx 5$.

To understand the behaviour seen in figure 22, we must examine the mechanism by which the oscillatory forcing remobilizes the droplet. A droplet which is trapped on the upstream side of the constriction must be displaced from its original position to a point just past the midpoint of the constriction. This distance is a function of the surface tension and the capillary geometry but scales linearly with the length scale L. For oscillatory forcing levels significantly above F_{plug}, the instantaneous droplet velocity is nearly proportional to F_ω even in the narrow constriction. The amplitude of the oscillatory displacement thus scales as $F_\omega\tau$. Equating this displacement with the distance required for remobilization yields a linear scaling for the critical frequency $L/U_1\tau \sim F_\omega$ which is consistent with the results shown in figure 22.

The simple analysis above assumes that the drop will be remobilized if the oscillatory displacement carries it past the midpoint of the constriction. This assumption is valid if the mean forcing level F_o is sufficient to prevent the drop from reversing its course during the negative portion of the forcing cycle. As the oscillatory force pushes the drop through the constriction, the mean force adds an additional displacement

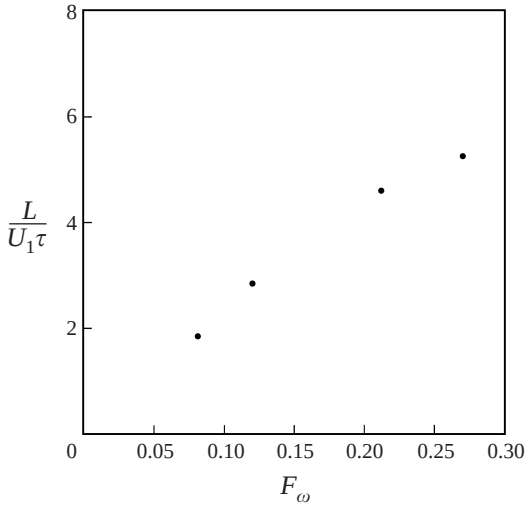

FIGURE 22. Critical frequency vs. oscillatory forcing level. Conditions are property number $Re/Ca = 0$, drop size $a/h = 2$, viscosity ratio $\lambda = 1$, density ratio $\rho_D = 1$, and $F_o = 0.03$.

proportional to $F_o\tau$. This extra displacement must exceed a certain fraction of L to prevent the reverse passage through the constriction. Owing to this constraint, the critical frequency levels off as shown in figure 22.

8. Unsteady simulations

The quasi-steady analysis has shown that large increases in the mean bulk flow rate and in the mean drop velocity are possible when oscillatory forcing is utilized. We have seen that the increase in flow rate is most pronounced when the steady driving force is below the pore-plugging threshold. Quasi-steady analysis predicts that a critical periodic frequency exists, above which oscillatory forcing is incapable of driving a droplet through a constriction. In this section we conduct full unsteady flow simulations with oscillatory forcing and compare the results with quasi-steady predictions. In the following, we will restrict ourselves to flows with $Re/Ca = 0$, and therefore the time scale for viscous diffusion $\rho h^2/\mu$ and the inertial response time of the droplet $\sqrt{\rho a^3/\gamma}$ are negligible.

In figure 23(a), we show the droplet position as a function of time for an unsteady simulation at low frequency $f = 0.00637$ ($L/U_1\tau = 2.21$) and compare with results based on quasi-steady analysis. The results show excellent agreement with only a slight variation as the droplet passes through each constriction. This figure illustrates a case where the periodic frequency is low enough for the oscillatory forcing to drive the drop through the constriction. The behaviour at higher frequencies is shown in figure 23(b), where we show the droplet positions for $f = 0.00127$ ($L/U_1\tau = 4.43$) as computed by unsteady simulations and by quasi-steady calculations.The agreement in this plot is excellent, demonstrating that quasi-steady analysis provides a good prediction of the unsteady forcing behaviour for frequencies above the critical frequency for droplet mobilization.

Finally, in figure 24, we show the critical frequency as a function of forcing level with results from quasi-steady analysis and from the full unsteady simulations. Again, there is good agreement, with the quasi-steady predictions deviating from

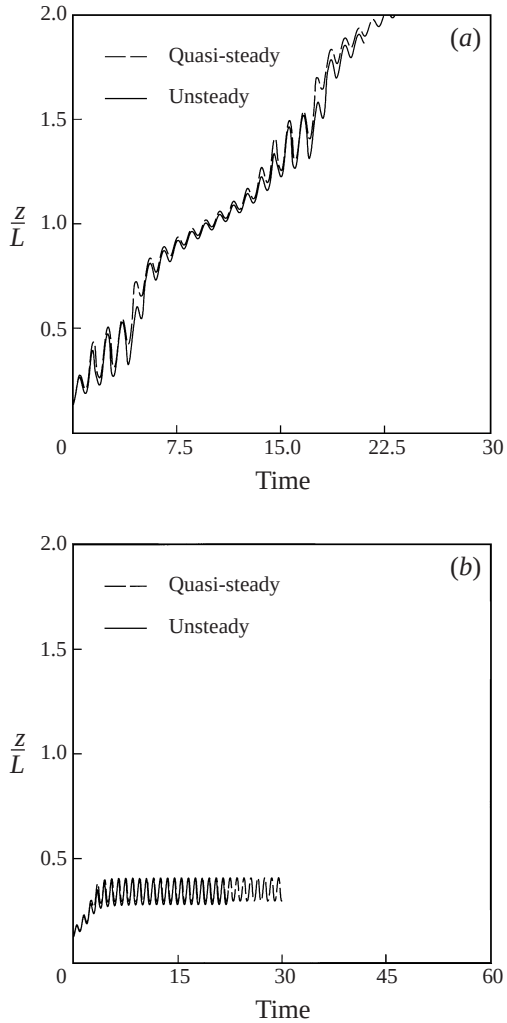

FIGURE 23. Comparison of droplet position vs. time at frequency (*a*) $L/U_1\tau = 2.21$ and (*b*) for a quasi-steady analysis and an unsteady simulation. Conditions are property number $Re/Ca = 0$, drop size $a/h = 2$, viscosity ratio $\lambda = 1$, density ratio $\rho_D = 1$, $F_o = 0.03$, and $F_\omega = 0.12$. Time is non-dimensionalized with the period of forcing τ.

the unsteady simulations only at the highest forcing level. With strong oscillatory forcing, the frequency f enters the range where the response time of the droplet is no longer fast enough for a quasi-steady analysis. We observe that the full unsteady simulation actually yields a *higher* critical frequency than the quasi-steady prediction. For frequencies just below the critical frequency, the droplet experiences an extra impulse as it pops through the constriction in the forward direction, but misses this extra push during the incomplete transit in the reverse direction. The unsteady simulation accurately resolves this directional bias, while the quasi-steady analysis fails to capture the phenomenon. Owing to this omission, the quasi-steady analysis gives a slight underprediction for the critical frequency in the high-frequency range.

The results presented in this section show that quasi-steady analysis can be employed to capture many features of unsteady, oscillatory flow. For the low Reynolds

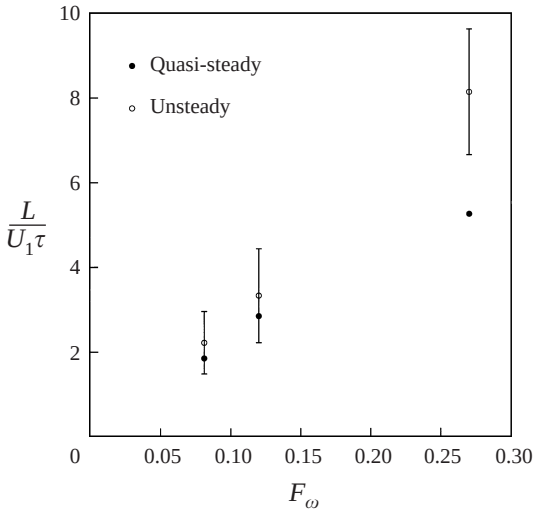

FIGURE 24. Critical frequency vs. oscillatory forcing level. Conditions are property number $Re/Ca = 0$, drop size $a/h = 2$, viscosity ratio $\lambda = 1$, density ratio $\rho_D = 1$, and $F_o = 0.03$. The error bars show the uncertainty in the critical frequency for the unsteady simulations.

number, low capillary number flows considered here, there is excellent agreement between the quasi-steady predictions and the unsteady simulations. For nearly all forcing levels considered, the quasi-steady analysis gives accurate predictions for the droplet motion over the relevant range of periodic frequency. The critical periodic frequency is predicted well by quasi-steady analysis. For frequencies above the critical value, oscillatory forcing is ineffective for remobilizing droplets, and the unsteady simulations required for this regime are of little interest. On a final note, we observe that unsteady simulations are likely to be more important for inertial flows at higher Reynolds numbers, or for higher capillary number flows where the drop response time is slower than the convective or oscillatory time scales.

9. Conclusions

We have analysed droplet flow through constricted tubes over a wide range of conditions for both constant and oscillatory forcing. For constant forcing, we have presented detailed computations of the drop shape, bulk flow rate and drop velocity and have determined the conditions for which droplets exhibit pore plugging. The critical force required to overcome pore plugging is found to be a strong function of the drop size a/h, while the dependence on fluid inertia Re/Ca and viscosity ratio λ is weaker. Our analysis of oscillatory forcing has shown that pore plugging plays an integral role in determining the mean flow rate. For systems with a relatively small mean force, a dramatic increase in mean flow rate occurs as the oscillatory forcing becomes strong enough to overcome the plugging threshold. Further increases in the oscillatory forcing level lead to small increases in mean flow rates.

The phenomena studied in this paper may be relevant to enhanced oil recovery operations which have demonstrated increased efficiency in the presence of acoustic stimulation. Owing to the predominance of surface tension forces in petroleum reservoirs, pore plugging is a common occurrence leading to trapped oil droplets and a reduction in the overall permeability of the medium. Our results show that

acoustic stimulation may be an effective means to remobilize some of these droplets, thereby increasing the oil recovery rate and enhancing the permeability of the media. The results in this paper may be applicable to other flows involving porous media in industrial operations. Examples include filtration, flow in packed beds and the manufacture of fibrous composites. In addition to these engineering applications, enhanced transport subject to oscillatory forcing may be important in the movement of blood cells through small blood vessels with constrictions. A cell which would plug the vessel under a weak steady pressure force may be remobilized with the large oscillatory forcing supplied by the circulatory system.

This work was supported by a grant from the National Science Foundation. D. R. G. acknowledges the support of a Computational Science and Engineering Fellowship from the University of Illinois. Computational resources were provided by IBM through the Shared University Resource Program at the University of Illinois, and by the National Center for Supercomputing Applications.

REFERENCES

Borhan, A. & Hemmat, M. 1997 Deformation of viscous drops in flow through sinusoidally constricted capillaries. In *Moving Boundaries IV Computational Modeling of Free and Moving Boundary Problems* (ed. R. Van Keer & C. A. Brebbia), pp. 275–284. Computational Mechanics Publications.

Gauglitz, P. A. & Radke, C. J. 1989 Dynamics of Haines jumps for compressible bubbles in constricted capillaries. *AIChE J.* **35**, 230–240.

Graham, D. R. 1997 Steady and oscillatory flow through model porous media. MS thesis, University of Illinois.

Graham, D. R. 1999 Acoustic stimulation of multiphase flow in porous media. PhD thesis, University of Illinois.

Graham, D. R. & Higdon, J. J. L. 2000 Oscillatory flow of droplets in capillary tubes, Part 1. Straight tubes. *J. Fluid Mech.* **425**, 31–53.

Hemmat, M. & Borhan, A. 1996 Buoyancy-driven motion of drops and bubbles in a periodically constricted capillary. *Chem. Engng. Commun.* **148–150**, 363–384.

Leyrat-Maurin, A. & Barthes-Biesel, D. 1994 Motion of a deformable capsule through a hyperbolic constriction. *J. Fluid Mech.* **279**, 135–163.

Martinez, M. J. & Udell, K. S. 1989 Axisymmetric creeping motion of drops through a periodically constricted tube. In *AIP Conf. Proc. 197 Drops and Bubbles*, pp. 222–234. American Institute of Physics.

Olbricht, W. L. & Leal, L. G. 1983 The creeping motion of immiscible drops through a converging/diverging tube. *J. Fluid Mech.* **134**, 329–355.

Tsai, T. M. & Miksis, M. J. 1994 Dynamics of a drop in a constricted capillary tube. *J. Fluid Mech.* **274**, 197–217.